UNLIMITED

(2)

RSRE
MEMORANDUM No. 4418

ROYAL SIGNALS & RADAR ESTABLISHMENT

FORWARD OPTICAL SCATTERING FROM VERY ROUGH SURFACES NEAR GRAZING INCIDENCE

Author: D L Jordan

PROCUREMENT EXECUTIVE,
MINISTRY OF DEFENCE,
RSRE MALVERN,
WORCS.

RSRE MEMORANDUM No. 4418

UNLIMITED

ROYAL SIGNALS AND RADAR ESTABLISHMENT

Memorandum 4418

Title: FORWARD OPTICAL SCATTERING FROM VERY ROUGH SURFACES NEAR GRAZING INCIDENCE

Author: D L Jordan

Date: August 1990

SUMMARY

A series of metal and dielectric targets exhibiting fractal characteristics are produced having a range of surface roughnesses between about 1μm and 16μm. They are all sufficiently rough that only diffuse reflection was obtained from them when illuminated with a He-Ne laser beam. The intensity scattered in the specular direction has been measured as a function of the surface roughness for near normal (θ_i = 20°) and near grazing (θ_i = 85°) incidence. The specular direction intensity at first falls rapidly with increasing surface roughness, but then saturates at high values of the surface roughness. Good agreement is obtained between the experimentally observed variation with surface roughness and that predicted theoretically using a fractal surface scattering model and surface parameters measured using a profile instrument. A simple graphical model is used to demonstrate qualitatively the trends observed.

RSRE MEMORANDUM No 4418

FORWARD OPTICAL SCATTERING FROM VERY ROUGH SURFACES NEAR GRAZING INCIDENCE

D L Jordan

CONTENTS

1. Introduction

The aim of this Memorandum is to present experimental results of He-Ne laser scattering near grazing incidence from surfaces that are very rough compared to the laser wavelength; for comparison results are also presented for near normal incidence. Only forward scattering is considered. Future work will concentrate on grazing angle backscatter geometries because of their relevance to high resolution radar scattering from the sea surface.

Little data exists on either forward grazing angle scattering or forward scattering from very rough surfaces. Work in the optical field has tended to concentrate on surfaces having roughness ranging from considerably less than, to slightly greater than the optical probing wavelength. This regime is of limited usefulness however for trying to elucidate some of the mechanisms responsible for observations made of radar scattering from the sea-surface. Examples of these are the ratio of vertical to horizontal polarised returns in backscatter and the variation of the returns with sea-surface roughness in both forward and backscatter geometries.

There is at present no universally accepted sea-surface model. However, one that has had some success in allowing some aspects of radar scattering from the sea to be predicted is the composite model[1]; this assumes the sea is composed of two different scales of waves which affect the radar cross-section in different ways. A spectrum of small capillary waves with amplitudes less than the radar wavelength is assumed which cause Bragg resonant scattering. These small capillary waves are in turn assumed to be distributed on larger facets which are tilted from the horizontal to represent the larger gravity waves or swell. Unfortunately this model fails to predict the ratio of vertical to horizontally polarised radar cross-sections observed from backscatter measurements[2]. Recently a sea-surface model based on a fractal geometry has been proposed. This is discussed in more detail in references 3 and 4. At present it appears that a fractal index

$\nu \sim 2$, corresponding to a marginal fractal may be realistic, at least for some sea surfaces.

In this Memorandum a series of surfaces having fractal properties with measured surface roughnesses ranging from just greater than the optical wavelength (λ = 0.6328 μm) to approximately 25λ are investigated. The surfaces are described in detail in section 2 and the scattering measurements in sections 3, 4 and 5. A comparison of the measured mean scattered intensity with theoretical predictions is made. The results of some simple graphical simulation are presented in section 6 as an aid to understanding the observed trends. Future work will attempt to produce two scale surfaces as well as fractal ones and determine their different scattering characteristics in both backscatter and forward scatter geometries.

2. Surface Preparation

A series of stainless steel targets of varying roughnesses were prepared by randomly pressing an engraving tool onto the metal. This technique has been previously shown[5] to produce a good approximation to a fractal surface over a wide range of scale sizes when applied to Germanium. By varying the pressure on the engraving tool the surface roughness could be varied. Unfortunately this technique naturally resulted in the surface height autocorrelation function ρ increasing with the surface roughness. No simple method could be found of independently varying the surface roughness and ρ over the range of roughnesses required.

Surface height profiles along one-dimensional scans across the surfaces were recorded using a 'Talysurf' stylus instrument. From these the surface structure function, defined as

$$S(\delta) = \langle [h(x) - h(x+\delta)]^2 \rangle \qquad (1)$$

where h is the local surface height at position x, was determined. For a fractal surface this is related to the two fractal parameters ν and L that completely describe it by

$$S(\delta) = L^{2-\nu} |\delta|^{\nu} \qquad (2)$$

The fractal index ν is related to the Hausdorff-Besicovitch dimension D of a section profile of the surface by $\nu = 2(2-D)$ and L is the topothesey; this is the length over which the rms slope difference is unity. From (2) it follows that a plot of log $S(\delta)$ verses log δ allows the determination of both ν and L. A typical structure function plot is shown in Figure 1; the straight line has been drawn through the experimental points for reference. It is obvious that the plot is linear over a range of scale sizes from $\sim 3\mu$m, which is the lower limit of resolution of the 'Talysurf' up to $\sim 70\mu$m. The limited horizontal resolution of the stylus instrument unfortunately precludes characterising the surface at scale sizes comparable to the optical probing wavelength of 0.633 μm. However there is no a-priori reason for assuming that the fractal regime indicated by the linear form of the log-log structure function does not extend down to this region; the scattering data presented later re-enforces this view. The slope of the straight line region gives ν and the intercept allows L to be determined.

A surface roughness parameter is invariably used when describing rough surfaces. Unfortunately such parameters are obviously beset with difficulties when applied to fractal surfaces. For example, the measured surface roughness is a function of the length over which it is measured. Nevertheless, because of the need to make comparisons with sea scattering data etc where the surface is described in such terms, the arithmetic average roughness R_a was measured for each surface with a small portable stylus instrument (Rank, Taylor, Hobson Surtronic); this measured R_a over a 5 mm length of surface and used a 0.8 mm cut-off. A relation between R_a and the fractal parameters ν and L is described in Section 5.

The arithmetic average roughness is defined for a profile length L (5 mm in these measurements) as

$$R_a = \frac{1}{L} \int_0^L |z| \, dx$$

where z is measured from the mean level. For a symmetrical Gaussian distribution of surface heights R_a is related to the rms surface roughness σ by

$$R_a = \left[\frac{2}{\pi} \right]^{\frac{1}{2}} \sigma \simeq 0.8\sigma$$

Surfaces were produced with R_a values of 0.92μm, 2.3μm, 4.7μm, 6.3μm, 6.6μm, 10.2μm and 15.5μm, covering the range $1.4 \leqslant R_a/\lambda \leqslant 24.5$. For all the samples the fractal index ν was approximately constant and equal to 1.66 ± 0.04. The topothesey however varied over quite a wide range; from 2 x 10^{-5} μm to 6.3 x 10^{-2} μm. All the samples possessed an isotropic surface.

The measured surface height histograms for surfaces with R_a = 2.3μm, 10.2μm and 15.5μm are shown in Figures 2(a), 2(b) and 2(c) respectively. The vertical axis is the number of points having heights (in arbitrary units) in the range given by the horizontal axis. Also shown for each one is a Gaussian distribution calculated using the measured mean and standard deviation. From these, which are typical of all the surface height histograms, it can be seen that at best the histograms are only very approximately fitted by Gaussian distributions. The measured Skewness(Sk) and Kurtosis(K) is shown for each one in the figures. For comparison an attempt to fit the histograms to a Gamma-distribution was also made. For this the height distribution is given by

$$p(h) = \left[\frac{m}{\langle h \rangle} \right]^m h^{m-1} \quad \frac{\exp \{ - mh/\langle h \rangle \}}{\Gamma(m)}$$

where the fitting parameter m was determined from the measured values of $\langle h^2 \rangle$ and $\langle h \rangle^2$ as

$$\frac{\langle h^2 \rangle}{\langle h \rangle^2} = 1 + \frac{1}{m}$$

As can be seen from Figures 2(a), 2(b) and 2(c) the resulting fit to the measured data was if anything, slightly worse than that obtained using a Gaussian distribution.
For comparison purposes a few surfaces were prepared using dielectric (perspex) rather than a metal. Three surfaces having R_a values of 0.75 μm, 5.8μm and 14.2 μm were made. The fractal index ν was rather higher in this case, being approximately 1.84 (± 0.03). L ranged from 1.3 x 10^{-4} to 4.2 x 10^{-12} μm.

3. Experiment

The experimental arrangement is shown schematically in Figure 3. The output from a polarised He-Ne laser was passed through a chopper, scattered from the target and detected by a 3 mm wide by 9 mm long photodiode. The output from the detector, togther with the chopper reference signal was connected to a Brookdeal 5209 Lock-in amplifier. All measured intensities are quoted in micro-volts. The detector was mounted on an arm that replaced the telescope on a divided circle spectrometer, the collimator arm

having been removed. The target was mounted on the prism table at the centre of the spectrometer. The detector to centre of target distance was ~ 370 mm.

The laser beam diameter was ~ 3.5 mm at the target position. Angles of incidence θ_i of greater than ~ 87° led to illuminated lengths comparable to the target size of 40 mm and so θ_i was limited to a maximum of 85°. Because of the relatively small illuminated size near normal incidence the experiments were repeated several times with the target moved between each measurement and the results averaged to ensure that a large proportion of the target was sampled. The targets were also rotated to ensure they were isotropic. Speckle averaging was automatically achieved by the use of a relatively large detector aperture (3 mm x 9 mm), the typical speckle size being of order 70 μm.

Measurements were carried out with the incident radiation either p or s polarised. P-polarised light has its electric field vector parallel to the plane of incidence and corresponds to V-polarised radiation in radar terminology; s-polarised light (H-polarised in radar) has its electric field vector perpendicular to the plane of incidence. Changes from one state of polarisation to the other were accomplished by rotating the cylindrically symmetrical laser in its mounting. The detection system was made polarisation sensitive by mounting a rotatable sheet polariser/analyser of extinction ratio approximately 400:1 in front of the photodiode.

4. Diffuse Reflection

To verify that the metal targets were actually acting as fractal scatterers the mean scattered intensity as a function of angle $\langle I(\theta)\rangle$ was measured for one particular target for angles of incidence θ_i of 20° and 85° and compared with that predicted from theory using 'Tallysurf' measured values of r and L. The target with R_a = 2.3 μm was used; for this surface r = 1.63 and L = 5 x 10^{-4} μm.

For a perfectly conducting isotropic two-dimensional fractal surface the diffusely scattered component is given by[6]

$$\langle I(\theta)\rangle \propto F^2(\theta) \int_0^\infty r\, J_0[krG(\theta)] \exp\left[-\tfrac{1}{4}k^2 f^2(\theta)\, L^{2-r}\, r^r\right] dr \qquad (3)$$

where various inessential angle-independent terms have been omitted. F, G and f are angle dependent terms given by

$$F(\theta) = \frac{1 + \cos\theta_1 \cos\theta_2 - \sin\theta_1 \sin\theta_2 \cos\theta_3}{\cos\theta_1 + \cos\theta_2} \qquad (4)$$

$$G(\theta) = \left[(\sin\theta_1 - \sin\theta_2 \cos\theta_3)^2 + \sin^2\theta_2 \sin^2\theta_3\right]^{\frac{1}{2}} \qquad (5)$$

$$f(\theta) = \cos\theta_1 + \cos\theta_2 \qquad (6)$$

where θ_1, θ_2, and θ_3 are as defined in Figure 4. For all the measurements described in this Memorandum θ_3 = 0.

Equation (3) should strictly be limited to situations where the Kirchoff approximation is valid i.e. to situations in which small angle scalar diffraction theory is valid. This of course is questionable for fractals because they include scale sizes less than the wavelength of the incident radiation. Provided however the scattering power of the inner scale sizes is small, by which is meant their rms 'height' is much smaller than a wavelength, then the basic scattering characteristics of the fractal model will be unaffected in near specular

directions. Small scale roughness will however contribute to large angle scattering and so some doubt exists as to the validity of Fraunhofer large angle scattering results obtained using a fractal model. There are also a number of other approximations implicit in using (3) at large scattering angles. These include neglect of the variation of reflectivity with angle, shadowing and polarisation effects which are obviously not included in the scalar treatment used here. However, in spite of these omissions there is an accumulating body of experimental evidence that exhibits trends consistent with those predicted by (3) even from multi-scale surfaces at relatively large scattering angles[5,6,7]. Near grazing angle results have not however previously been published.

The variation of $<I(\theta)>$ with scattering angle θ for $\theta_i = 20^\circ$ and 85° is shown in Figures 5 and 6 respectively; angles are measured from the normal to the mean target surface. Also shown are the curves calculated from (3) using the measured values of ν and L. In both figures the theoretical curve has been normalised to the mean of the measured p and s-polarised returns at $\theta = 38^\circ$. The good agreement in shape between the measured and calculated curves is readily apparent. In both cases the calculated curve underestimates the measured values near the specular direction, and this is discussed more fully later. It also fails at angles above about 85° for the $\theta_i = 20^\circ$ case due to the lack of any shadowing correction in (3). A simple shadowing correction that has been successfully used before is outlined in reference 6. The good agreement between the form of the calculated and measured angular variations of the scattered diffuse intensity, even at near grazing incidence lends support to the contention that the metal surfaces do indeed behave as fractal scatterers with the measured values of ν and L.

5. Specular Reflection

The variation of the mean intensity scattered in the specular direction $<I(\theta_s)>$ with surface roughness R_a is shown in Figure 7 for $\theta_i = 20^\circ$ and Figure 8 for $\theta_i = 85^\circ$. There is very little difference between the p and s-polarised results for $\theta_i = 20^\circ$; nearer grazing incidence ($\theta_i = 85^\circ$) however the s-polarised signal is consistently higher than the p-polarised one for all values of R_a by a factor of 3 to 4. This is purely a manifestation of the different behaviour of the Fresnel reflection coefficients for p and s-polarised radiation with angle, and is determined not by the surface roughness but by the complex refractive index of the metal target. This is illustrated in Figure 9 which shows the variation of the specular signal with angle of incidence for the smoothest metal surface investigated ($R_a = 0.9\ \mu m$). It shows there is very little difference between the p and s-polarised signals at $\theta_i = 20^\circ$, but at 85° the s-polarised signal is about 3.5 times that of the p-polarised one. As grazing incidence is approached the p and s-polarised returns became closer to each other.

The results shown in Figures 7 and 8 for both angles of incidence show that the reduction of specular direction intensity with increasing surface roughness levels-off at large values of R_a, the effect being more noticeable for the large angle of incidence case. Some simple graphical modelling to show the physical basis for this behaviour is presented in Section 6.

For all the targets investigated in this work the surface constitutes a very rough target ($(4\pi/\lambda)\sigma \cos\theta_i > 1$) even at angles of incidence of 85°. Consequently a true specular component is unlikely; the reflected radiation in the specular direction should be diffusely reflected. Therefore equation (3) may be expected to be appropriate and can be evaluated analytically in the specular direction for arbitrary values of ν and L as

$$<I(\theta_s)> \propto F^2(\theta) \frac{\Gamma\left\{\frac{2}{\nu}\right\}}{\nu\left[\frac{1}{2}k^2 f^2(\theta)\, L^{2-\nu}\right]^{2/\nu}} \qquad (7)$$

The values calculated using this expression are shown superimposed on the measured values in figures 7 and 8 and marked 'Theory'. As with the calculations of the angular variation of scattered radiation shown in Figures 5 and 6, the results have been scaled by an appropriate factor to bring them into agreement with the measured values. This is

necessary because of the omission of various inessential angle independent factors in (3). The reason for the difference in scaling factor between the specular and non-specular cases remains obscure. It is obvious from Figs. 5 and 6 that the scaling factor required to fit the data away from the specular direction underestimates the specular direction values. However, the excellent agreement shown in Figs 7 and 8 between the measured specular direction values and those calculated using an appropriate scaling factor strongly suggests that (7) is correct. Work by Kim et al[9] indicates that for diffusers with Gamma distributed surface profiles the specular component is much higher than expected. Experimentally they observed a specular component with He-Ne laser radiation when the standard deviation of the surface height fluctuations was as high as 2μm from a target possessing a negative exponential surface height distribution. However the surface height histograms shown in Figure 2 do not appear to be obviously Gamma-distributed and so the reason for this behaviour remains unresolved at present.

Traditionally measurements of surface structure are made in terms of the surface roughness σ and the surface height correlation length ζ, not in terms of fractal parameters. Because a simple finite scale model behaves like a fractal at small displacements a correspondence may be drawn between such models and fractal ones. For any model possessing a Lorentzian spectrum and surface rough enough to produce large phase fluctuations on reflection, it can be shown that for two-dimensional isotropic surfaces

$$L^{2-D} = \frac{2\sigma^2}{\zeta^D} \quad \ldots \quad (8)$$

Assuming a Gaussian height distribution σ can be expressed in terms of R_a as $\sigma = 1.25\ R_a$. For the surfaces studied in this work the surface height correlation length ζ varies linearly with R_a as shown in Figure 10. i.e. $\zeta = 4R_a + B$. Substituting this in (8) leads to the following expression for the topothesey in terms of D and R_a as

$$L = 2^{\frac{1}{(2-D)}} (1.25)^{\frac{2}{2-D}} \frac{R_a^{\frac{2}{2-D}}}{(4R_a + B)^{\frac{D}{2-D}}} \quad (9)$$

From Fig 10, A = 5.5 and B = 12 μm. The variation of L with R_a calculated from (9) is shown in Figure 11 and is in reasonable agreement with the values determined from the structure function plots.

A similar variation of the specular intensity with surface roughness to that found from the metal targets was observed using the perspex ones; these are shown in Figure 12. For ease of following the trends a continuous curve has been drawn through each set of results. As expected the biggest difference between the results obtained using the metal and dielectric targets is in terms of the degree of cross depolarisation observed. This is defined (as a percentage) as the ratio of the signal detected with the polariser/analyser orthogonal to that emitted by the laser, to that with it parallel to the emitted polarisation direction. Some results for the metal target are shown in Figure 13; to make the plots easier to read the measurements at discrete angles have been replaced by continuous curves. Depolarisation is shown plotted against angle for two angles of incidence (20° and 85°) for s and p-polarisation of the laser. As seen, the degree of depolarisation is quite small, ranging from 1% or less near the specular direction to a maximum of about 10% well away from it. The values obtained well away from the specular direction are possibly an overestimate as the depolarised component was very small and comparable to the system noise level. For the perspex targets the degree of depolarisation near the specular direction was again of order 1% or less, but in this case rose to very high values away from it as shown in Figure 14. For example for p-polarised light the depolarisation approached 100% as expected at the Brewster angle (~ 56°).

Work in the microwave radar field on near grazing angle forward scatter had led to the suggestion[10] that a form of roughness parameter defined as ($\sigma \cos \theta_i/\lambda$) may be useful. The suggestion is that if the surface roughness σ and the angle of incidence θ_i are varied so as to maintain $\sigma \cos \theta_i$ constant, the scattering signal should remains constant unless shadowing is important. It may therefore be used to estimate the importance of shadowing. A brief attempt has been made to check this idea. Figure 15 is a plot of the specular intensity from the metal targets as a function of R_a for $R_a \cos \theta_i/\lambda = 1.45$. The lowest R_a surface corresponds to an angle of incidence of 20° and the highest one to $\theta_i = 82°$. The same data is shown plotted as a function of the angle of incidence in Figure 16. Obviously the specular direction signal is far from constant as the angle of incidence and surface roughness is varied. Although the data is very limited and any conclusions drawn must be tentative ones, Figure 16 suggests that the specular direction signal may be relatively constant from low angles of incidence, up until perhaps 60°–70°; beyond this the signal fails off markedly. Similar results were obtained for $R_a \cos\theta/\lambda = 2.1$. Care must be exercised in transferring these tentative findings directly to the radar situation because of differences in radar transmitter and receiver antennae gains, and optical detector field of view compared to the illuminated target region. For example, as grazing angle is approached the illuminated patch becomes extremely long and may well exceed the receiver field of view. More work is planned in this area to clarify some of the uncertainties.

6. Graphical Simulation

As a simple aid to understanding the reasons for the fall-off and saturation of the specular direction intensity with increasing surface roughness a simple graphical approach was adopted. A rough surface profile was generated on a computer from a sum of sinusoidal waves and the effect of varying the roughness monitored. Initially a sum of equally phased large scale-size waves of the same amplitude was used; figure 17 shows such a profile. The amplitude A is given by

$$A = 150 + \alpha (\sin 3x + \sin 1.5x + \sin x + \sin 0.75x + \sin 0.5x) \qquad (10)$$

A histogram of the surface height distribution is shown in figure 18 for $\alpha = 10$. Also shown is a Gaussian distribution of the same mean and standard deviation as the measured one. Because of the equality of the phases of the component waves the surface heights are not truly Gaussian distributed; this is also true for the actual metal and perspex surfaces described earlier (Figure 2). The e^{-1} correlation length was 46. As expected, the structure function plot for this surface indicated a fractal index of ~ 2 and a topothesey of approximately zero as shown in Figure 19.

As specular reflection only occurs from small regions or facets having zero slope, the specular intensity was taken as the number of points on the profile having a slope less than some arbitrary value; in this case less than one degree. Using this criterion the effect of varying α and hence the surface roughness on the specular intensity is shown in Figure 20 for three angles of incidence. It is immediately obvious that the same general trend of an initially rapid fall-off of intensity with increasing roughness, as was seen with the actual rough surface measurements is observed. The reduction in specular intensity with increasing σ is greatest for the largest angles of incidence, and is due to shadowing. The effect on the surface slope distribution of increasing the surface roughness is shown in Figure 21, and demonstrates the very large reduction in the number of low slopes as the surface roughness is increased.

Another way of dramatically affecting the surface slope distribution is to add a high frequency component to the wave structure. This is also a possible model for waves on the sea surface. To this end the wave given by (10) was modified by the addition of components of ten times the spatial frequency of those in (10) to

$$A(x) = 150 + \alpha\,(\sin 3x + \sin 1.5x + \sin x + \sin 0.75x + \sin 0.5x) + \alpha/4\,(\sin 30x + \sin 15x + \sin 10x + \sin 7.5x + \sin 5x) \quad (11)$$

Such a surface with $\alpha = 10$ is shown in Figure 22. The much more irregular appearance of this surface profile compared to the original shown in Figure 17 is immediately apparent. The effect of adding the high frequency components on the structure function of the original low frequency waves is shown in Figure 19. The normalised surface height autocorrelation function of the large scale waves, small scale ones and their sum is shown in figure 23. The effect on the surface slope distribution is given in Figure 24, and shows a similar effect to increasing the roughness of the large scale only waves. The variation of specular intensity with surface roughness is shown in Figure 25. At normal incidence the effect of adding the high frequency waves is to significantly reduce the signal. At larger angles of incidence the effect is very dramatic and illustrates quite well the major influence that small amplitude high frequency waves superimposed on large scale waves have on the specular direction scattering properties.

7. Conclusions

The experimental measurements made utilising very rough surfaces that exhibit fractal properties show that the intensity scattered in the specular direction decreases with increasing roughness, and in fact saturates at sufficiently high values of roughness. This is in qualitative agreement with observations obtained using microwave forward scattering from the sea surface close to grazing incidence. Elementary graphical analysis suggests this is due to a reduction in the probability of finding zero slope regions on the profile. Although this concept is strictly only valid for non-fractal surfaces, in practice it may be expected to give a reasonable guide to the behaviour for values of the fractal index of order two. At angles of incidence greater than about sixty degrees shadowing becomes increasingly important. The only signficant difference observed between relatively good conductors and dielectrics was in the degree of cross depolarisation produced.

Future experiments are planned in which both the targets characterised in this work, and hopefully targets containing two dominant scale sizes will be investigated in a backscattering configuration. This will allow comparisons to be made with microwave radar measurements of internal wave wakes.

Acknowledgements

The author is grateful for discussions on microwave radar aspects of this work with Dr C. J. Baker and for helpful discussions with Dr E. Jakeman.

References

1. Wright, J.W.; 1968, IEEE Trans, AP-16, No 2, 217.

2. Holliday, D; St-Cyr, G.J.; De Raad, Jr, L.L.; Woods, N.E; 1989 RDA-TR-146600-004,

3. Jordan, D.L.; 1990, RSRE Memorandum 3699.

4. Glazeman, R.F.; Weichmann, P.B.; J. Geophysical Res. to be published.

5. Jordan, D.L.; Hollins, R.C.; Jakeman, E.; 1983, Appl. Phys B, 31, 179.

6. Jordan, D.L.; 1990 RSRE Memo 4348.

7. Jordan, D.L.; Hollins, R.C.; Jakeman, E.; Prewett, A.; 1988, Surface Topography, 1, 27.

8. Beckmann, P.; Spizzichino, A.; The Scattering of Electromagnetic Waves from Rough Surfaces (Pergarmon Press, Oxford, 1963).

9. Kim, M.J.; Mendez, E.R.; O'Donnell, K.A.; 1987, J.Modern Optics, 34, No 8, 1107

10. Baker, C.; Private Communication.

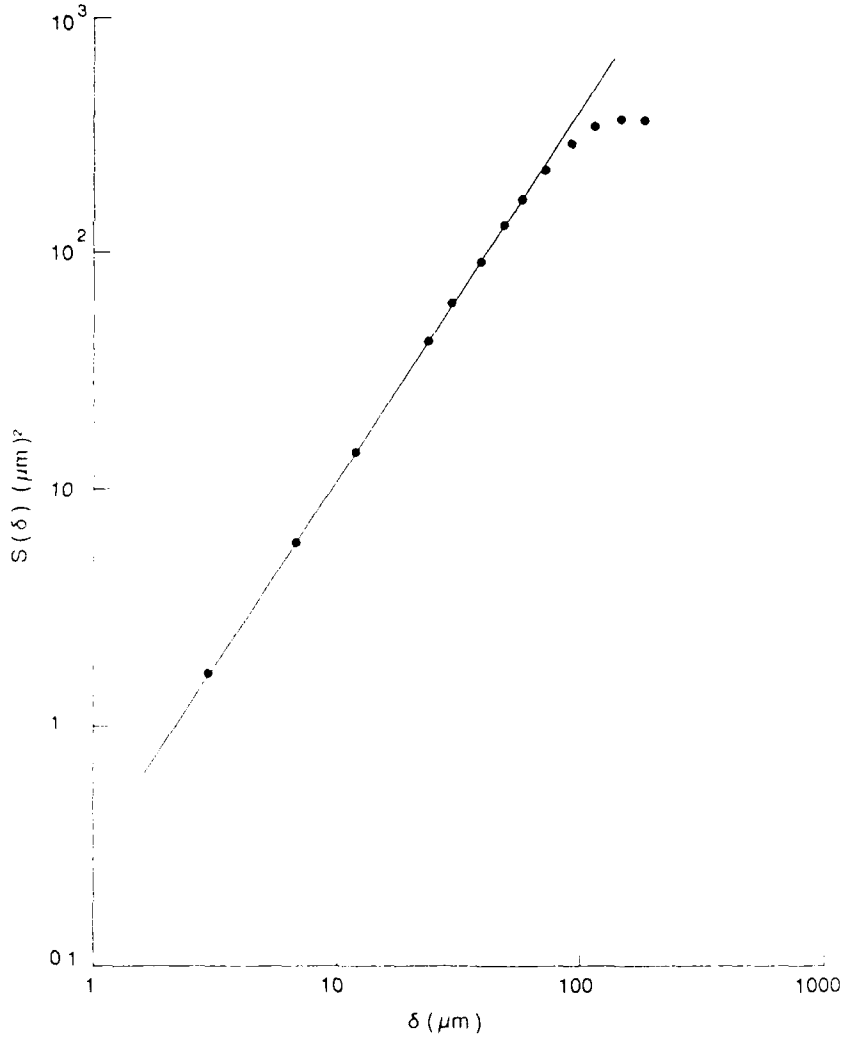

FIG 1. TYPICAL STRUCTURE FUNCTION PLOT

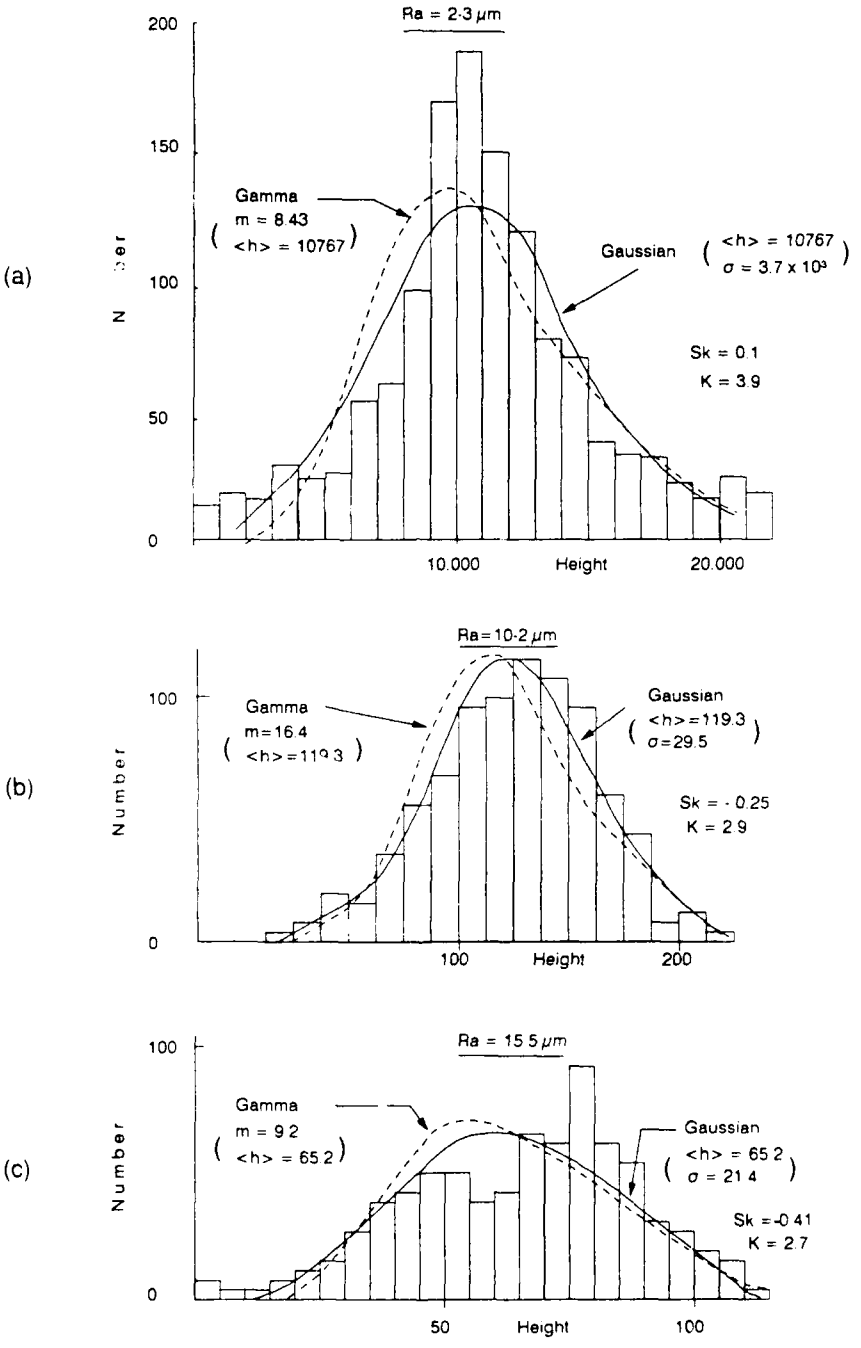

FIG 2. SURFACE HEIGHT HISTOGRAMS

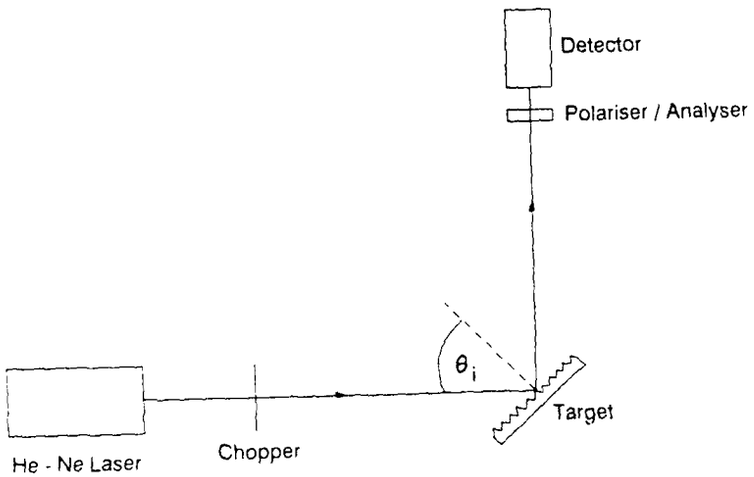

FIG 3. EXPERIMENTAL ARRANGEMENT

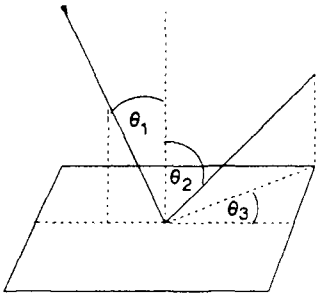

FIG 4. GEOMETRY FOR SCATTERING FROM A ROUGH SURFACE

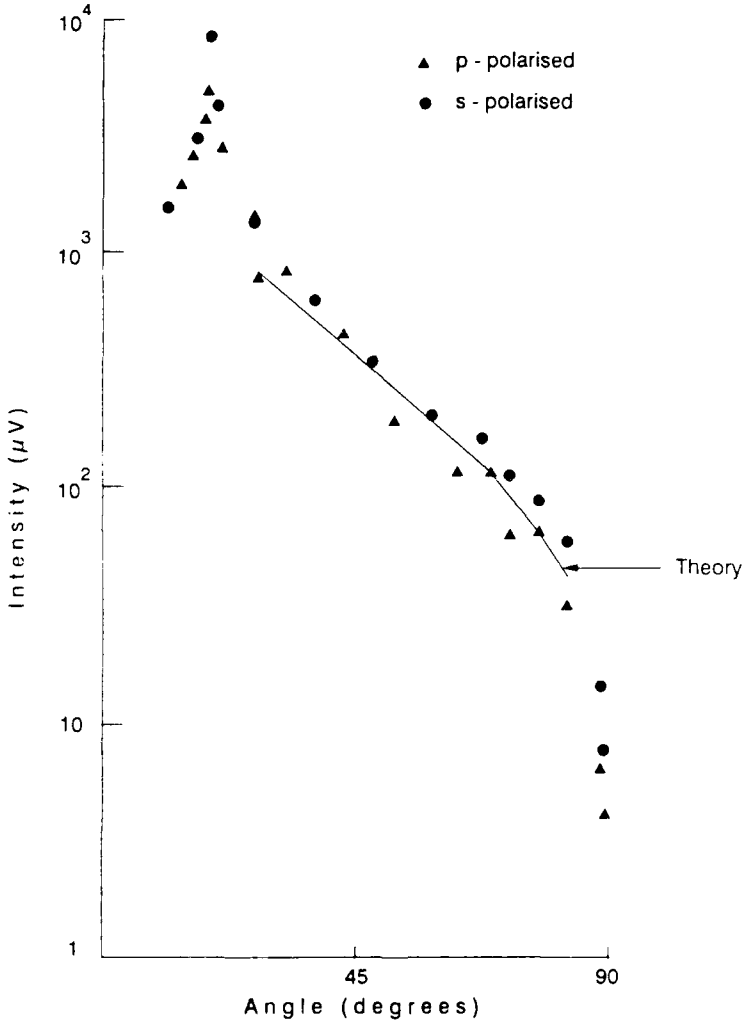

FIG 5. VARIATION OF SCATTERED INTENSITY WITH ANGLE FOR $\theta_i = 20^\circ$

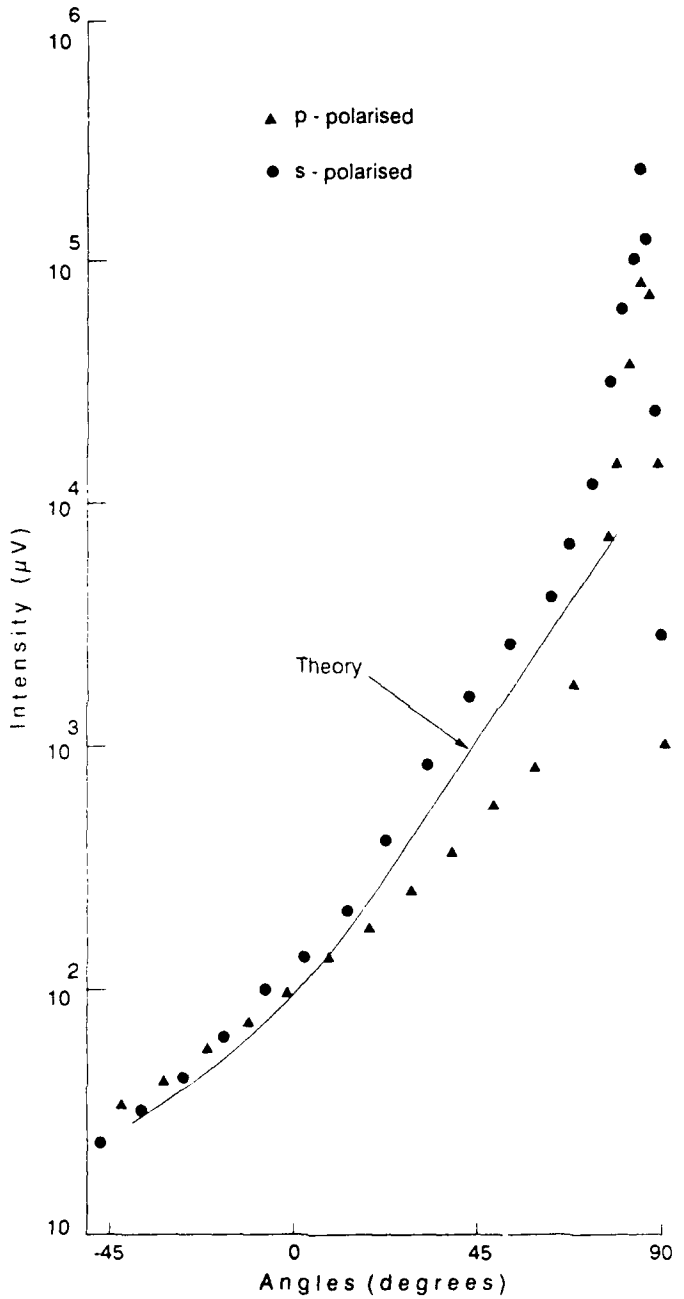

FIG 6. VARIATION OF SCATTERED INTENSITY WITH ANGLE FOR $\theta_i = 85^\circ$

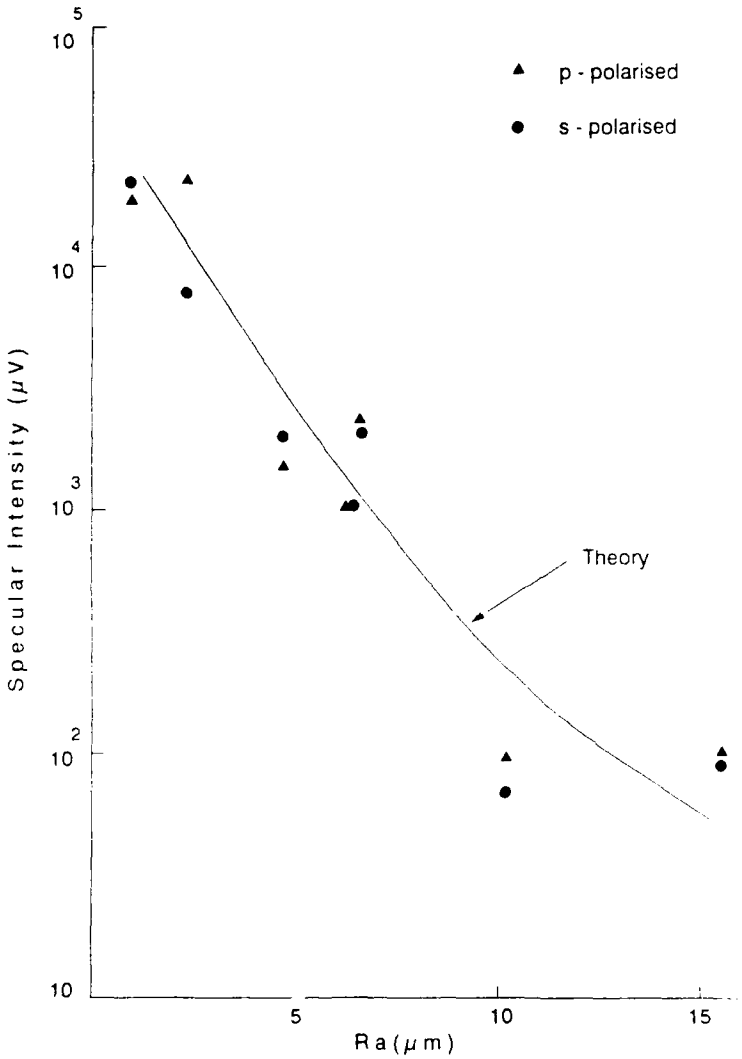

FIG 7. VARIATION F SPECULAR INTENSITY WITH SURFACE ROUGHNESS FOR $\theta_i = 20^\circ$. THEORY IS CALCULATED FROM (7)

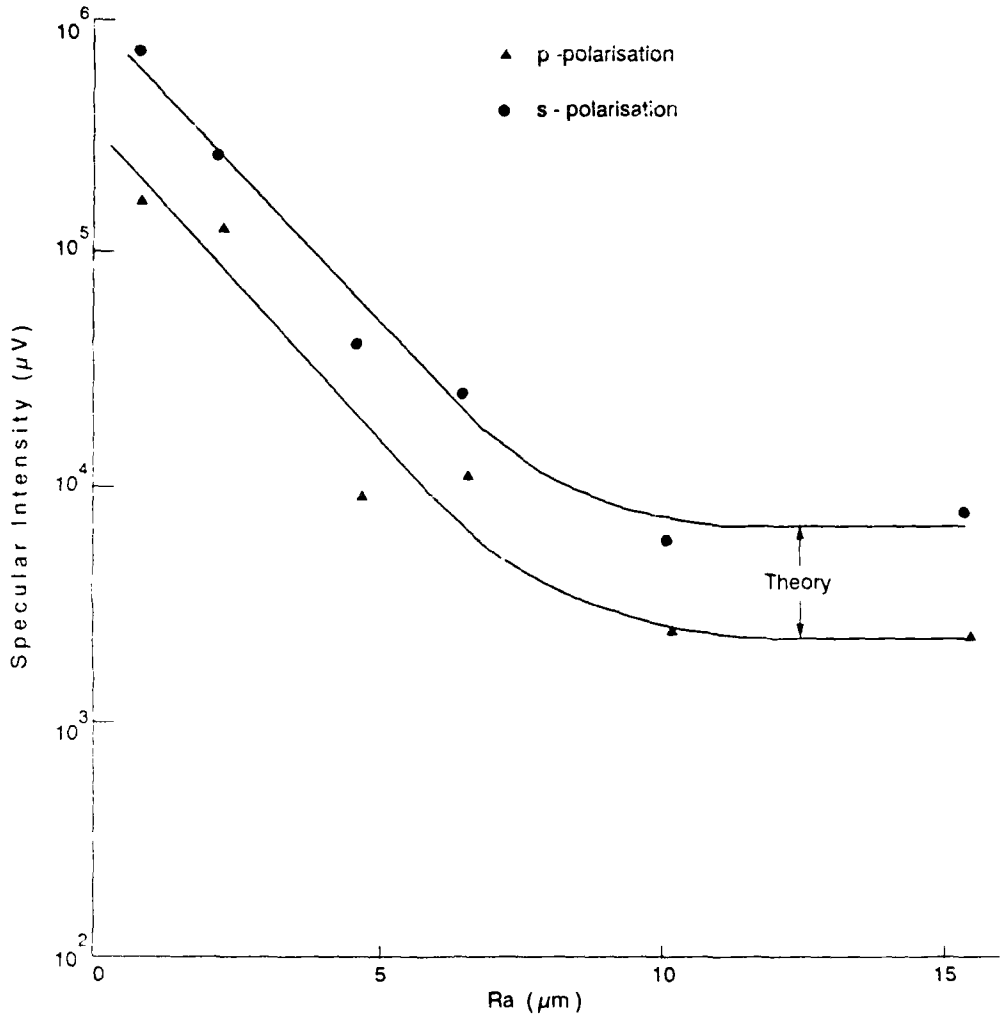

FIG 8. VARIATION OF SPECULAR INTENSITY WITH SURFACE ROUGHNESS FOR $\theta_i = 85^\circ$. THEORY IS CALCULATED FROM (7)

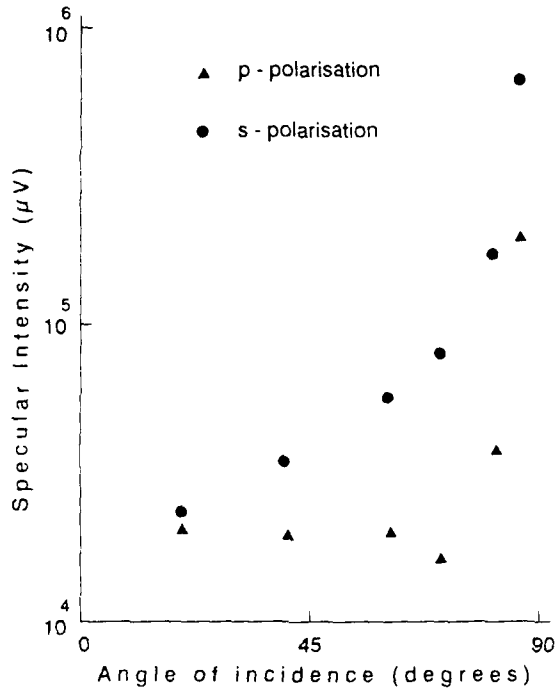

FIG 9. VARIATION OF SPECULAR REFLECTION WITH ANGLE OF INCIDENCE FROM SMOOTHEST METAL SURFACE

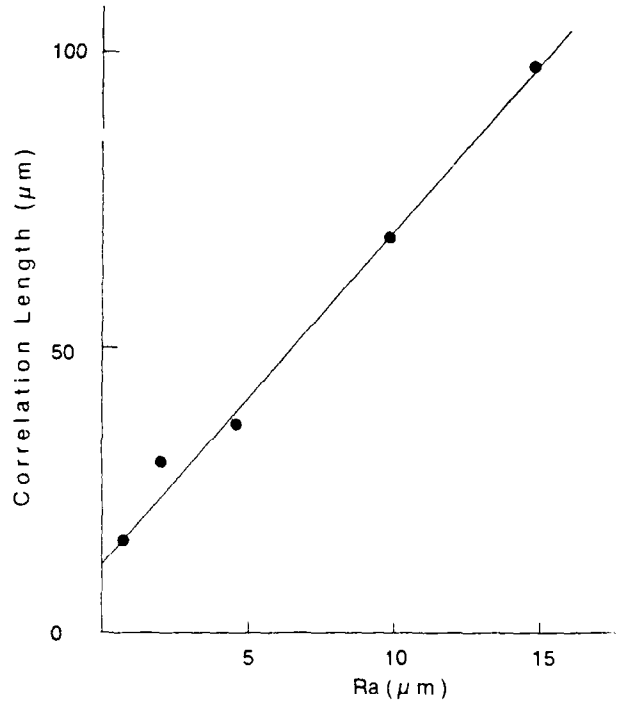

FIG 10. VARIATION OF SURFACE HEIGHT CORRELATION LENGTH WITH SURFACE ROUGHNESS

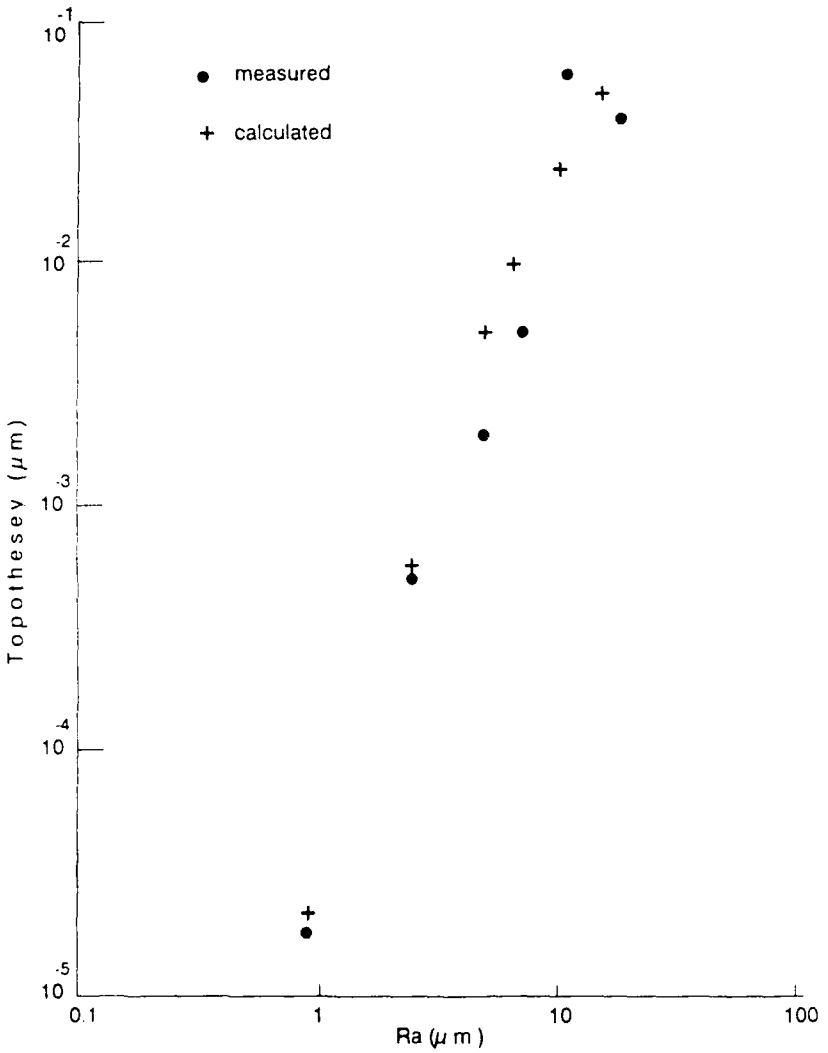

FIG 11. MEASURED AND CALCULATED VALUES OF THE TOPOTHESEY L AS A FUNCTION OF SURFACE ROUGHNESS

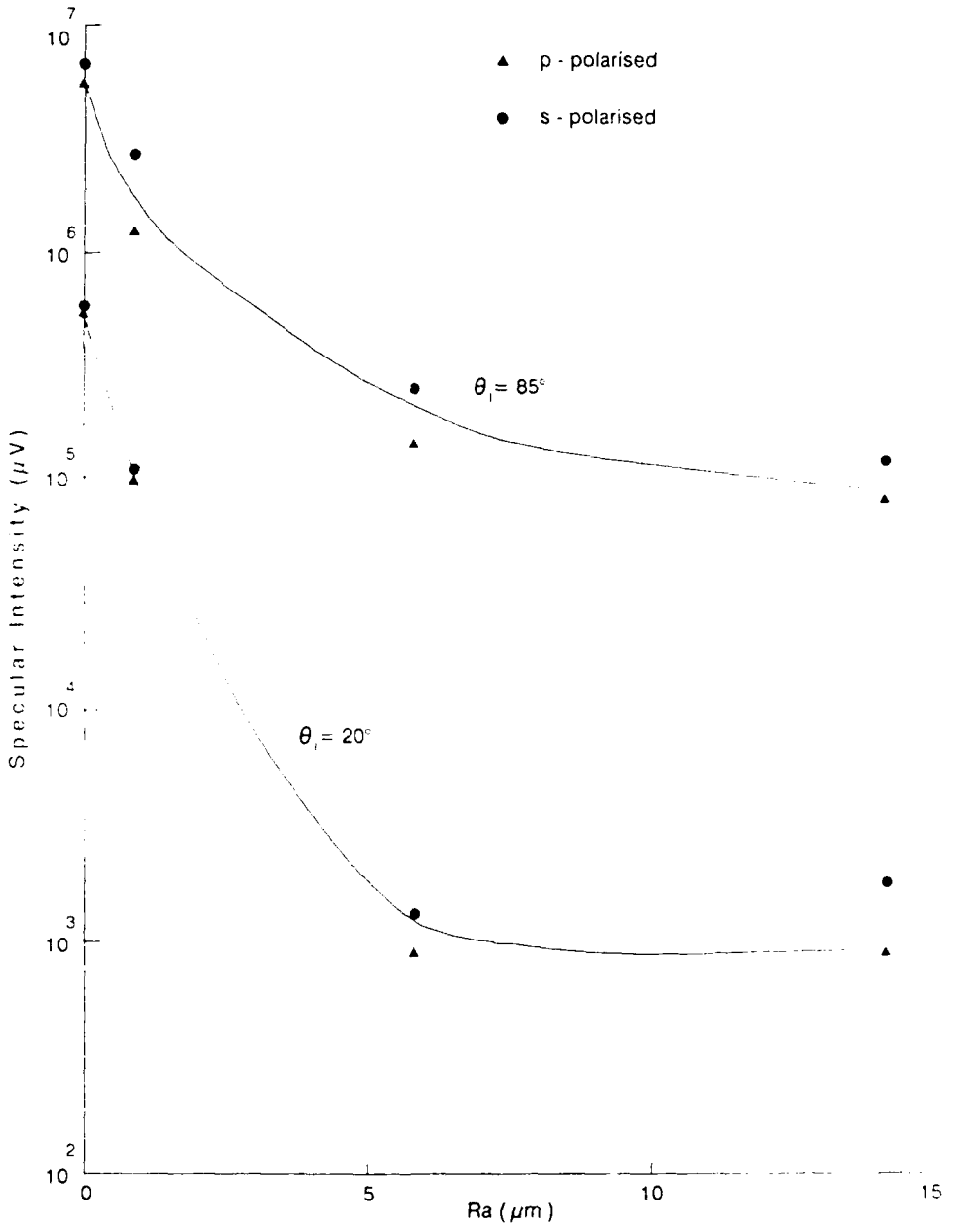

FIG 12. VARIATION OF SPECULAR DIRECTION INTENSITY WITH SURFACE ROUGHNESS USING PERSPEX TARGETS. THE CONTINUOUS CURVES ARE PURELY AN AID TO VIEWING THE GRAPH

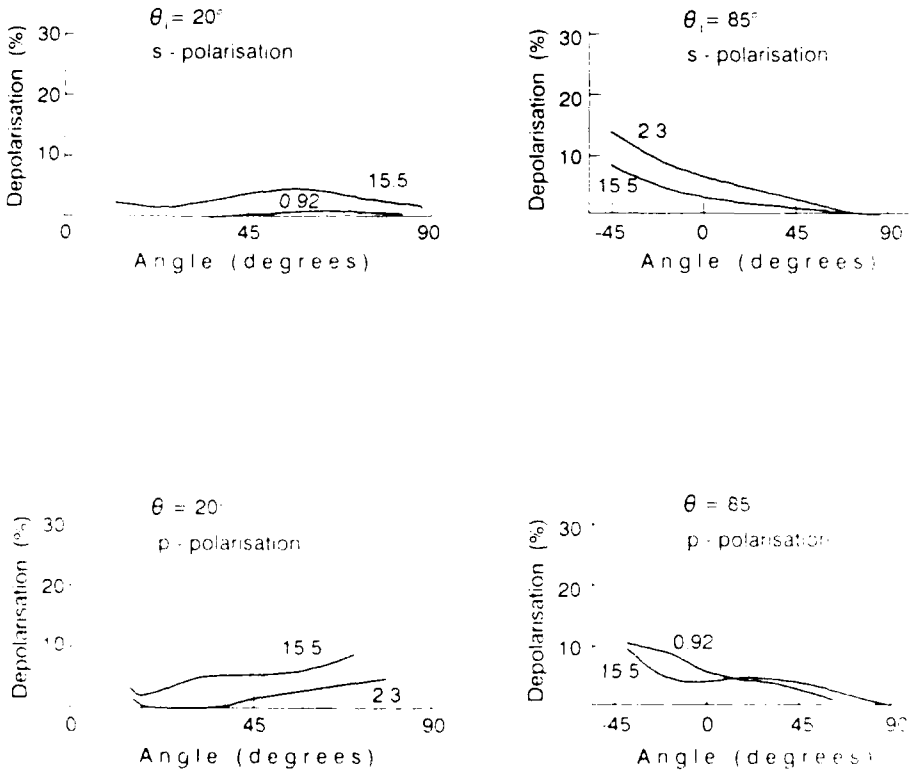

FIG 13. DEPOLARISATION FROM METAL TARGETS. FIGURES ON THE CURVES ARE THE SURFACE ROUGHNESS R_a

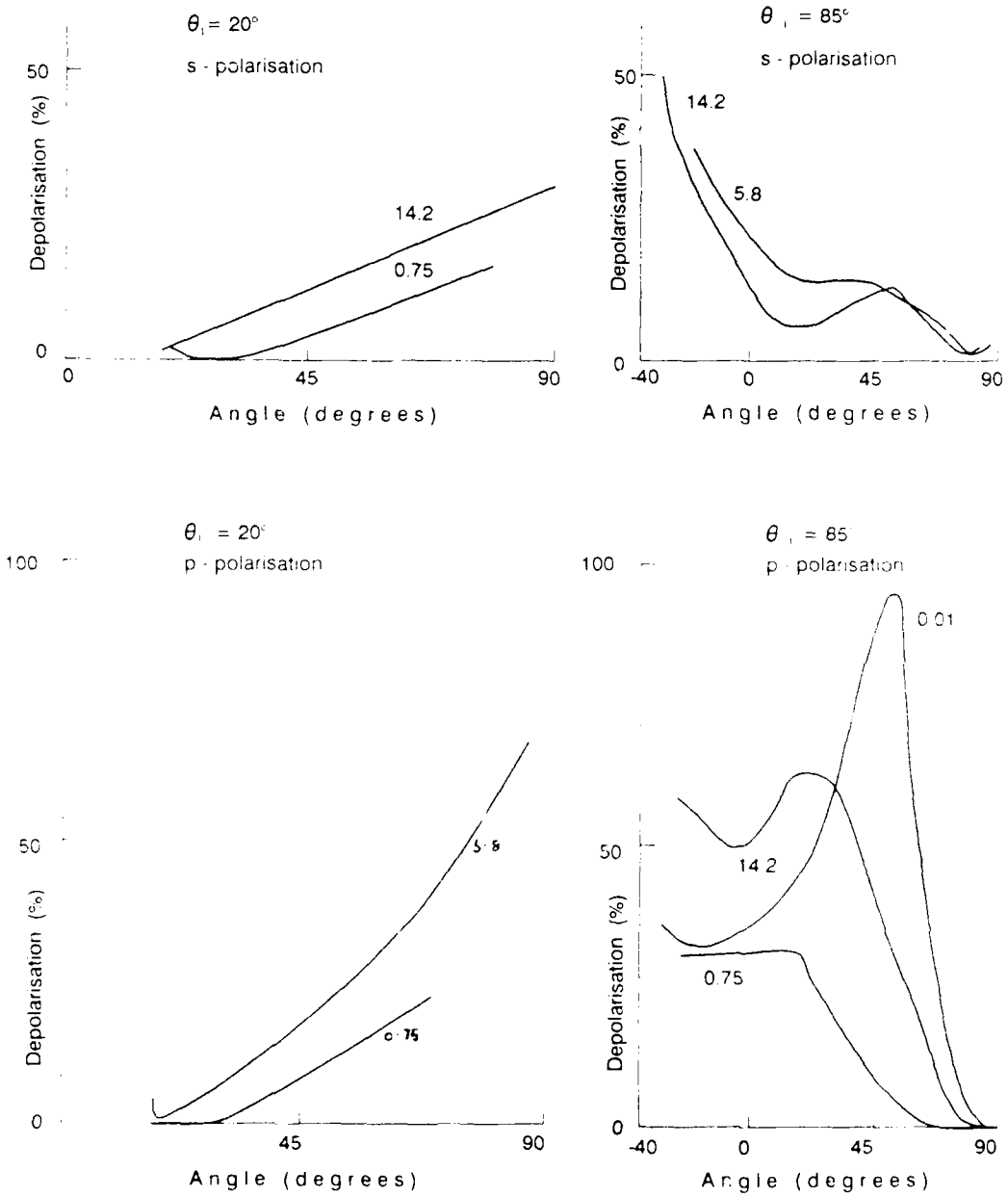

FIG 14. DEPOLARISATION FROM METAL TARGETS. FIGURES ON THE CURVES ARE THE SURFACE ROUGHNESS R_a

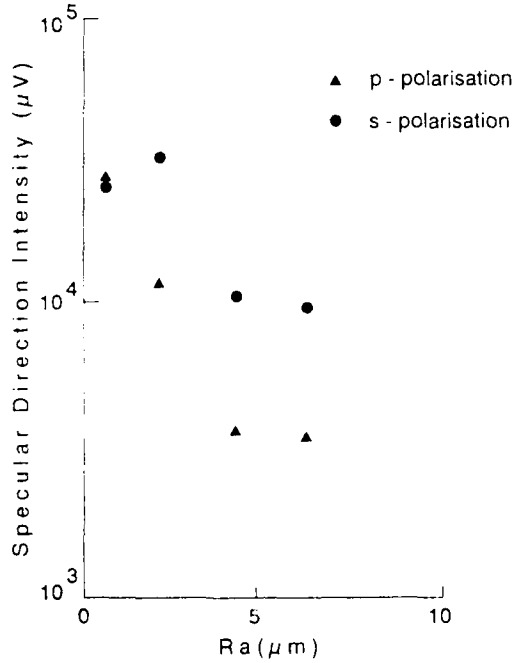

FIG 15. VARIATION OF SPECULAR DIRECTION SIGNAL WITH SURFACE ROUGHNESS FOR $(R_a \cos \theta_i)/\lambda = 1.45$

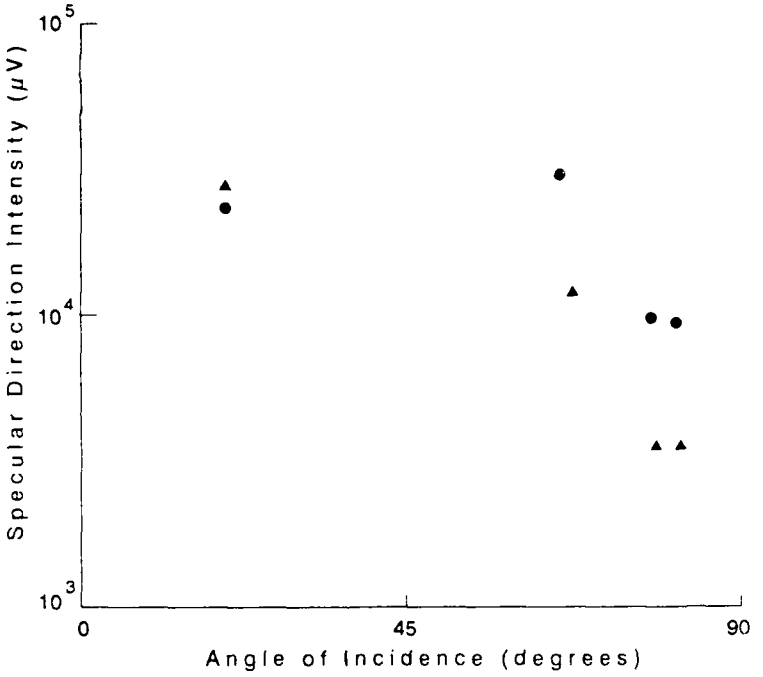

FIG 16. VARIATION OF SPECULAR DIRECTION SIGNAL WITH ANGLE OF INCIDENCE FOR $(R_a \cos \theta_i)/\lambda = 1.45$

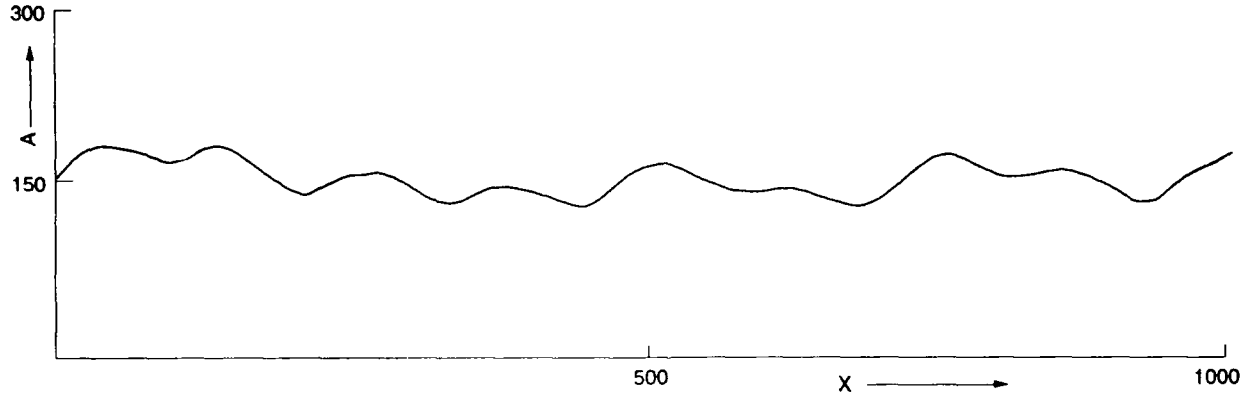

FIG 17. SURFACE PRODUCED USING LARGE SCALE SIZES ONLY

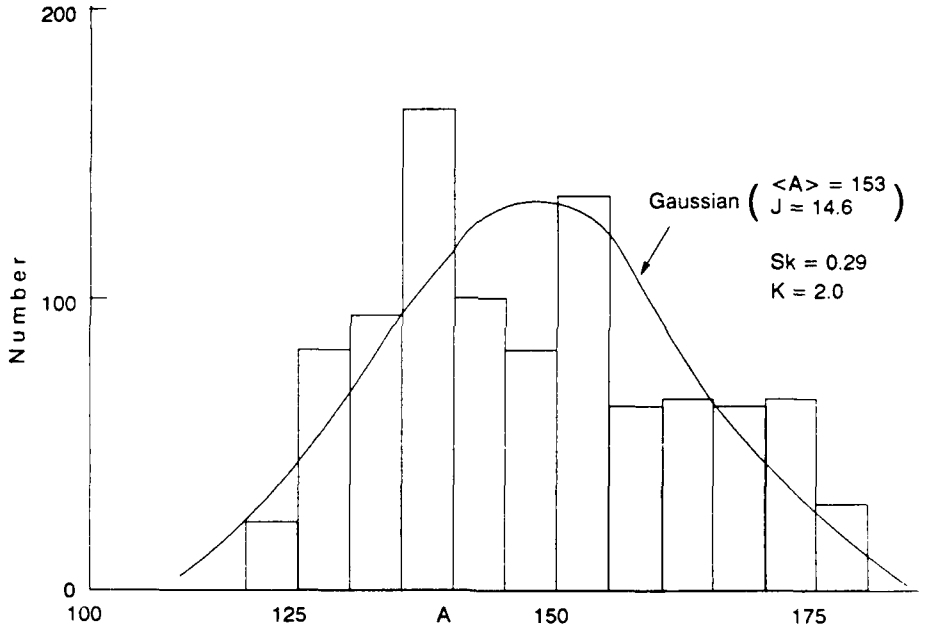

FIG 18. HEIGHT HISTOGRAM FOR SURFACE SHOWN IN FIGURE 17

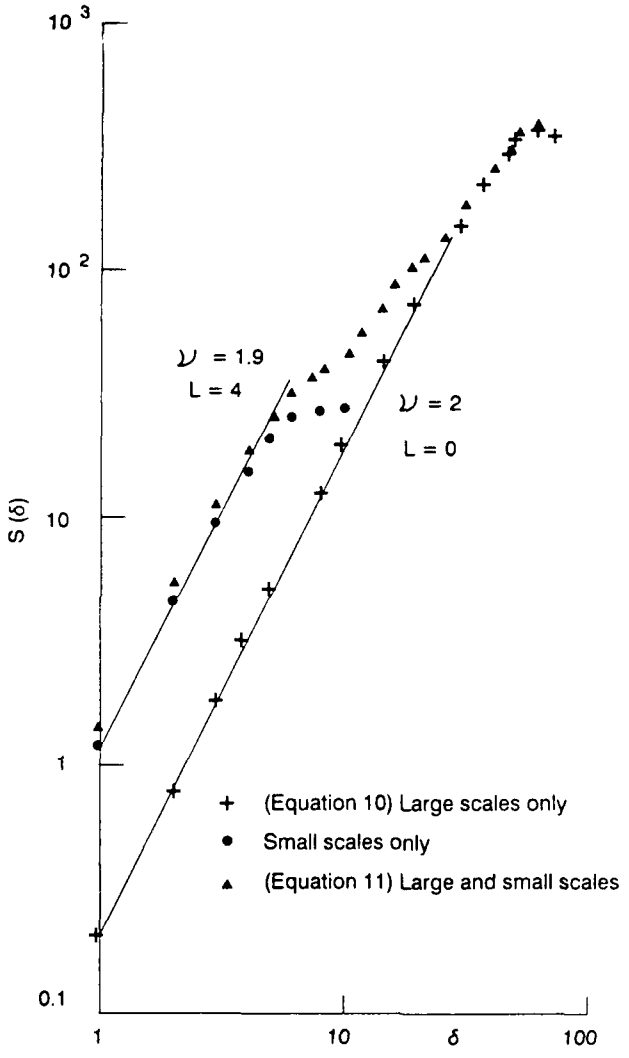

FIG 19. STRUCTURE FUNCTION PLOT FOR SURFACES ($\alpha = 10$) COMPOSED OF LARGE SCALES ONLY, SMALL SCALES ONLY AND COMPOSITE LARGE AND SMALL SCALES

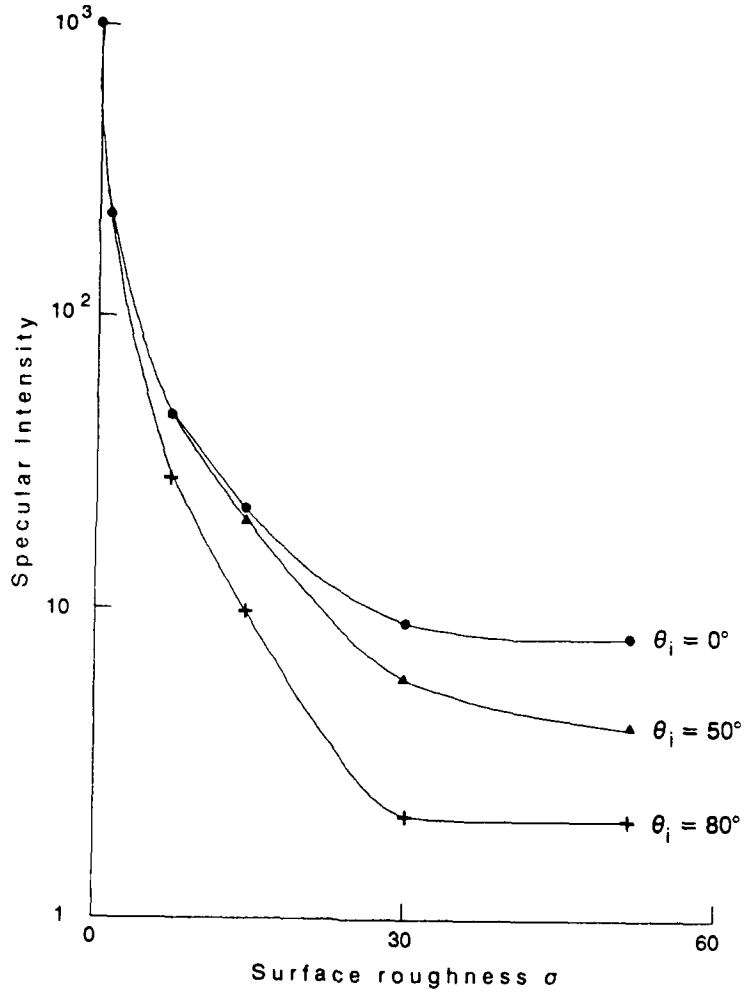

FIG 20. EFFECT OF SURFACE ROUGHNESS ON SPECULAR INTENSITY FOR SURFACE COMPOSED OF LARGE SCALE SIZES ONLY AND SHOWN IN FIGURE 17

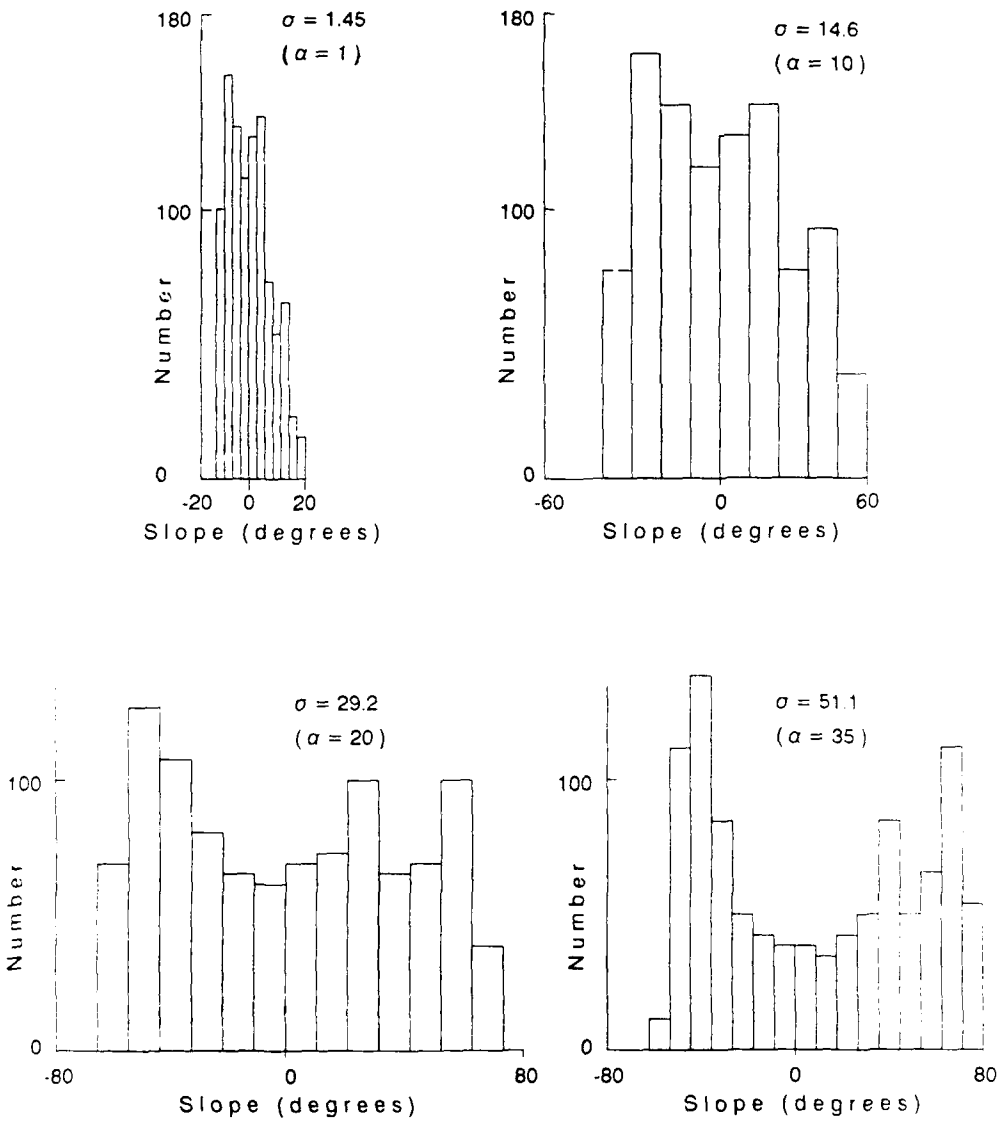

FIG 21. EFFECT OF SURFACE ROUGHNESS ON SLOPE DISTRIBUTION OF LARGE SCALE SIZES ONLY SURFACE

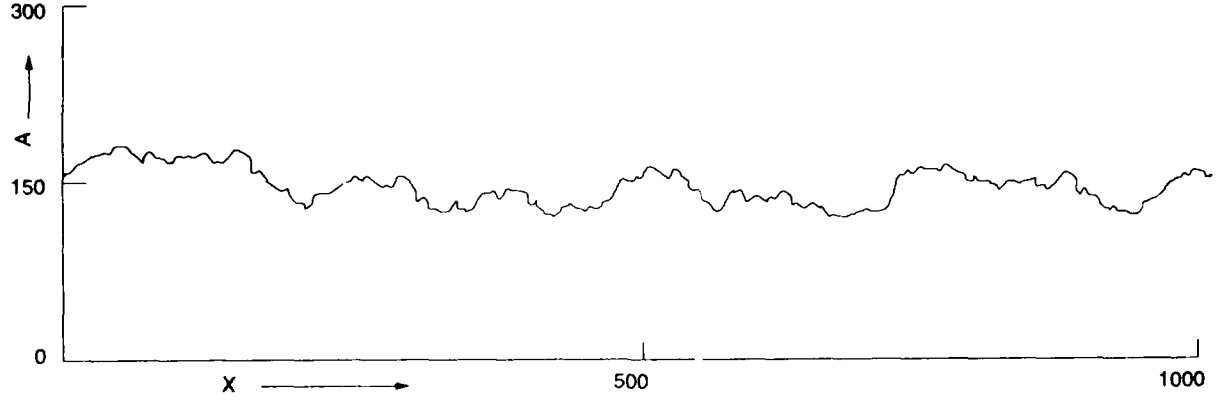

FIG 22. SURFACE PRODUCED USING BOTH LARGE AND SMALL SCALES

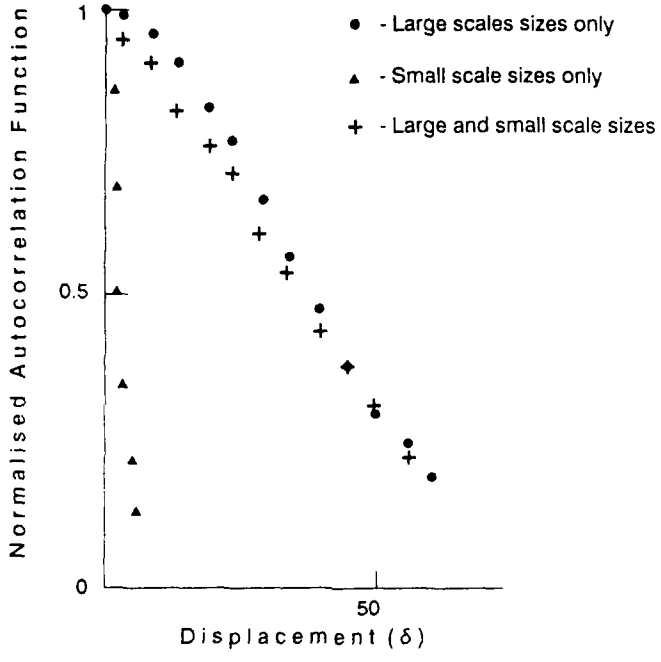

FIG 23. NORMALISED SURFACE HEIGHT SPATIAL AUTOCORRELATION FUNCTIONS FOR SURFACES CONTAINING LARGE SCALE SIZES ONLY (10), SMALL SCALE SIZES ONLY, AND BOTH LARGE AND SMALL SCALE SIZES (11). FOR ALL SURFACES $\alpha = 10$.

(a)

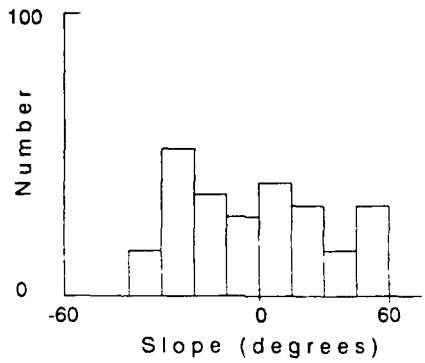

(b)

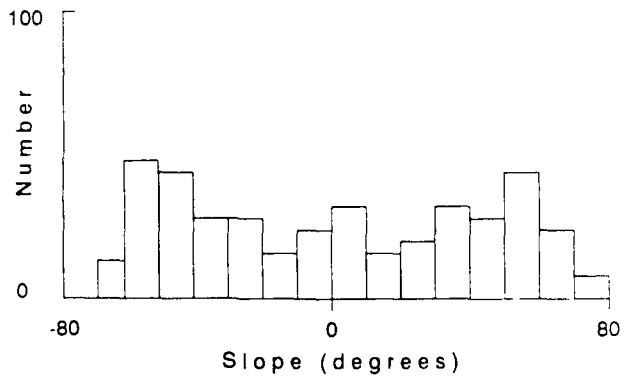

FIG 24. EFFECT ON SURFACE SLOPE DISTRIBUTION OF ADDING HIGH SPATIAL FREQUENCY COMPONENTS
a) LARGE SCALE SIZES ONLY ($\alpha = 10$)
b) LARGE AND SMALL SCALE SIZES ($\alpha = 10$)

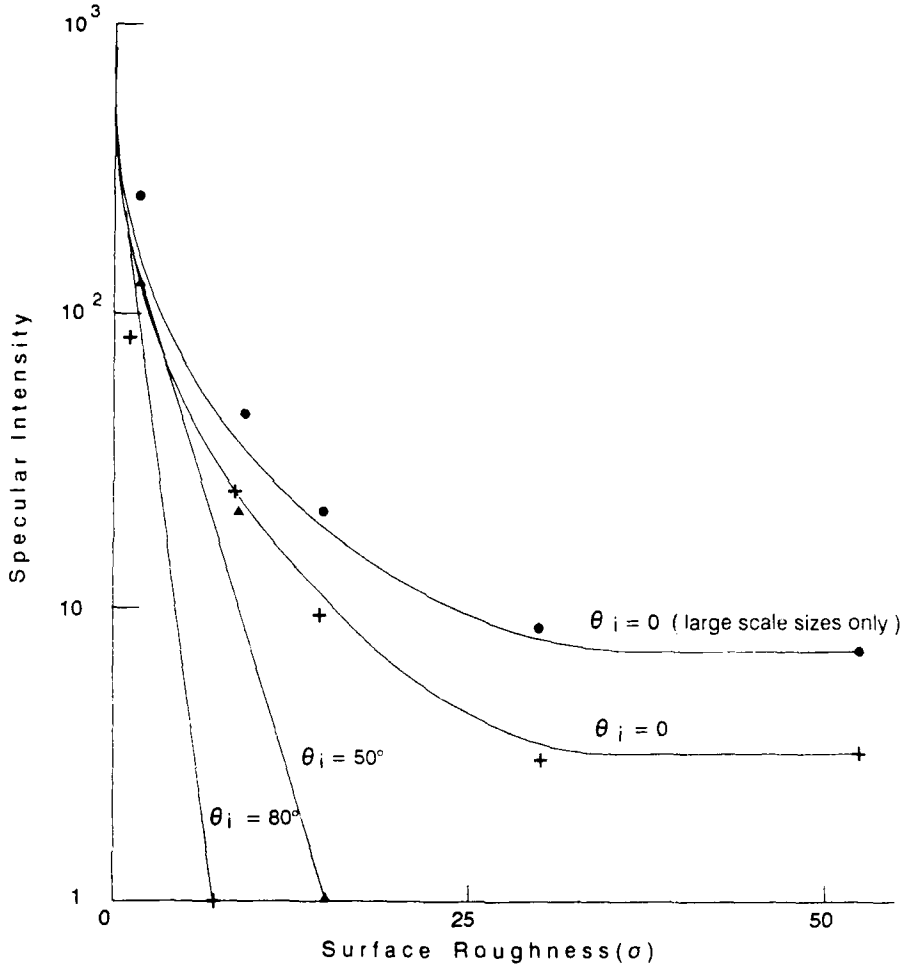

FIG 25. VARIATION OF SPECULAR DIRECTION INTENSITY WITH SURFACE ROUGHNESS FOR VARIOUS ANGLES OF INCIDENCE θ_i. SURFACE IS COMPOSED OF LARGE AND SMALL SCALES

REPORT DOCUMENTATION PAGE

DRIC Reference Number (if known) .....

Overall security classification of sheet .....UNCLASSIFIED.....
(As far as possible this sheet should contain only unclassified information. If it is necessary to enter classified information, the field concerned must be marked to indicate the classification eg (R), (C) or (S).

Originators Reference/Report No.	Month	Year
MEMO 4418	AUGUST	1990

Originators Name and Location
RSRE, St Andrews Road
Malvern, Worcs WR14 3PS

Monitoring Agency Name and Location

Title
FORWARD OPTICAL SCATTERING FROM VERY ROUGH SURFACES NEAR GRAZING INCIDENCE

Report Security Classification	Title Classification (U, R, C or S)
UNCLASSIFIED	U

Foreign Language Title (in the case of translations)

Conference Details

Agency Reference	Contract Number and Period

Project Number	Other References

Authors	Pagination and Ref
JORDAN, D L	11 + Diag

Abstract

A series of metal and dielectric targets exhibiting fractal characteristics are produced having a range of surface roughnesses between about 1 μm and 16 μm. They are all sufficiently rough that only diffuse reflection was obtained from them when illuminated with a He-Ne laser beam. The intensity scattered in the specular direction has been measured as a function of the surface roughness for near normal (θ_i=20°) and near grazing (θ_i = 85°) incidence. The specular direction intensity at first falls rapidly with increasing surface roughness, but then saturates at high values of the surface roughness. Good agreement is obtained between the experimentally observed variation with surface roughness and that predicted theoretically using a fractal surface scattering model and surface parameters measured using a profile instrument. A simple graphical model is used to demonstrate qualitatively the trends observed.

Abstract Classification (U,R,C or S)
U

Descriptors

Distribution Statement (Enter any limitations on the distribution of the document)
UNLIMITED